Arctic Sea Ice Variability in the Context of Recent Atmospheric Circulation Trends

CLARA DESER

National Center for Atmospheric Research, Boulder, Colorado*

JOHN E. WALSH

Department of Atmospheric Sciences, University of Illinois, Urbana–Champaign, Urbana, Illinois

MICHAEL S. TIMLIN

CIRES–Climate Diagnostics Center, University of Colorado, Boulder, Colorado

(Manuscript received 2 August 1998, in final form 9 March 1999)

ABSTRACT

Forty years (1958–97) of reanalysis products and corresponding sea ice concentration data are used to document Arctic sea ice variability and its association with surface air temperature (SAT) and sea level pressure (SLP) throughout the Northern Hemisphere extratropics. The dominant mode of winter (January–March) sea ice variability exhibits out-of-phase fluctuations between the western and eastern North Atlantic, together with a weaker dipole in the North Pacific. The time series of this mode has a high winter-to-winter autocorrelation (0.69) and is dominated by decadal-scale variations and a longer-term trend of diminishing ice cover east of Greenland and increasing ice cover west of Greenland.

Associated with the dominant pattern of winter sea ice variability are large-scale changes in SAT and SLP that closely resemble the North Atlantic oscillation. The associated SAT and surface sensible and latent heat flux anomalies are largest over the portions of the marginal sea ice zone in which the trends of ice coverage have been greatest, although the well-documented warming of the northern continental regions is also apparent. The temporal and spatial relationships between the SLP and ice anomaly fields are consistent with the notion that atmospheric circulation anomalies force the sea ice variations. However, there appears to be a local response of the atmospheric circulation to the changing sea ice cover east of Greenland. Specifically, cyclone frequencies have increased and mean SLPs have decreased over the retracted ice margin in the Greenland Sea, and these changes differ from those associated directly with the North Atlantic oscillation.

The dominant mode of sea ice variability in summer (July–September) is more spatially uniform than that in winter. Summer ice extent for the Arctic as a whole has exhibited a nearly monotonic decline (-4% decade^{-1}) during the past 40 yr. Summer sea ice variations appear to be initiated by atmospheric circulation anomalies over the high Arctic in late spring. Positive ice–albedo feedback may account for the relatively long delay (2–3 months) between the time of atmospheric forcing and the maximum ice response, and it may have served to amplify the summer ice retreat.

1. Introduction

Sea ice is a sensitive component of the climate system, influenced by conditions in both the atmosphere and ocean. Variations in sea ice may in turn modulate climate by altering the surface albedo; the exchange of heat, moisture, and momentum between the atmosphere and ocean; and the upper ocean stratification in areas of deep water formation. The surface albedo effect is considered to be one of the dominant factors in the poleward amplification of global warming due to increased ''greenhouse gas'' concentrations simulated in many climate models (e.g., IPCC 1990; Manabe et al. 1992; Randall et al. 1998).

Observational studies of sea ice extent indicate that variability on timescales of weeks and longer tends to be organized into large-scale geographical patterns that are closely associated with the dominant structures of atmospheric circulation variability, particularly during winter (Walsh and Johnson 1979; Overland and Pease 1982; Fang and Wallace 1994; Slonosky et al. 1997; Prinsenberg et al. 1997). The consensus of the observational studies is that ''interannual variability in sea ice conditions is caused by the variability in the large-

* The National Center for Atmospheric Research is sponsored by the National Science Foundation.

Corresponding author address: Dr. Clara Deser, NCAR/CGD, P.O. Box 3000, Boulder, CO 80307-3000.
E-mail: cdeser@ncar.edu

scale atmospheric circulation which locally manifests itself as surface air temperature and wind anomalies'' (Prinsenberg et al. 1997). Feedbacks or other influences of winter ice anomalies upon the atmosphere have been more difficult to detect due to the dominance of atmospheric forcing of sea ice in the observed associations, as shown by temporal asymmetries in ice–atmosphere cross-correlation functions (e.g., Lemke et al. 1980).

Over the past 3–4 decades, the dominant patterns of wintertime atmospheric circulation variability in the Northern Hemisphere, particularly the Pacific–North American and the North Atlantic oscillation (NAO) or Arctic oscillation (AO) teleconnection patterns, have exhibited trends that are unprecedented in the observational record. (For the purposes of this study, the NAO may be regarded as a subset of the spatially broader AO; see Thompson and Wallace 1998). Sea level pressures (SLPs) have decreased over the central Arctic and over the climatological Icelandic and Aleutian low centers, and increased farther south (Hurrell 1996; Thompson and Wallace 1998). The most pronounced SLP reductions over the central Arctic have occurred since 1988 (Walsh et al. 1996). Associated with these circulation changes, winter surface air temperatures over land (Eurasia in particular) have increased to record values while those over the oceans have cooled slightly (Hurrell 1996; Thompson et al. 2000). The latter authors hypothesize that anthropogenic forcing may be a contributing factor to the recent unprecedented strengthening of the polar vortex (reflected by the AO) and associated warming over the Northern Hemisphere continents.

Trends in Arctic sea ice extent have been evaluated most recently by Chapman and Walsh (1993), Maslanik et al. (1996), and Cavalieri et al. (1997). Sea ice cover over the Arctic as a whole has decreased by 2.9% per decade during 1979–96 (Cavalieri et al. 1997), with the largest reductions (6% decade^{-1}) in summer (Maslanik et al. 1996) and negligible change in winter. A similar seasonal dependence was reported by Chapman and Walsh (1993) for Arctic sea ice trends during 1961–90. Although winter ice extent for the Arctic as a whole has remained relatively stable, large trends of opposing sign are apparent in different regions, both for the more recent 1979–96 period (Parkinson et al. 1999, their Plate 2) and for several preceding decades (Chapman and Walsh 1993, their Fig. 9). Regionally, the magnitudes of the sea ice trends are as large in winter as in summer.

The purpose of this study is to examine the interannual variations in winter Arctic sea ice extent within the context of the recent hemispheric changes in atmospheric circulation and surface air temperature (SAT) during the last 40 yr (1958–97). Specifically, we address the following three questions.

- How are the temporal and spatial patterns of ice variability related to those of SAT and atmospheric circulation?
- Do the ice changes represent a response to the recent trends in atmospheric circulation and SAT?
- Is there any discernible influence of the ice cover variations upon the atmosphere?

We also examine Arctic sea ice variability during summer and its relation to spring atmospheric circulation changes. While earlier work has addressed the trends of Arctic sea ice coverage (e.g., Lemke et al. 1980; Chapman and Walsh 1993; Parkinson et al. 1999), the present analysis extends these earlier studies by quantitatively relating the sea ice variations to the large-scale atmospheric circulation. Moreover, the examination of cyclone variations in the context of a possible feedback from sea ice has not previously been undertaken with data of the past several decades. Finally, the evaluation of the linkage between summer and winter sea ice, particularly with regard to forcing by the winter–spring circulation, may be regarded as an original feature of this study.

2. Data and methods

a. Sea ice concentration

We use an updated version of the monthly mean sea ice concentration dataset (on a 1° lat × 1° long grid for the period 1953–97) described in Chapman and Walsh (1993). This dataset combines conventional estimates with microwave measurements from polar-orbiting satellites since 1972. The data sources and processing techniques are summarized in Chapman and Walsh (1993); the update is from satellite passive microwave data provided by the National Snow and Ice Data Center (NSIDC 1998). The sea ice concentration record exhibits a discontinuity in October 1978 associated with a change in the satellite sensor and passive microwave retrieval algorithm that depicts lower concentrations within the pack ice during during the melt season (April–September; see appendix). For this reason, we shall present results based upon the full period of record for the winter (January–March) season only; for the summer (July–September) season, we carry out a separate analysis for the periods before and after 1978. Since the correlations between the winter time series of ice concentration and ice extent exceed 0.9 in the Beaufort, Greenland, and Labrador Seas (not shown), the conclusions obtained here are insensitive to the choice of concentration rather than extent as the primary sea ice variable for the winter season. Similar results are found for summer.

b. NCEP reanalyses of surface air temperature and surface sensible and latent heat flux

Four times daily values of surface air temperature, sea level pressure, and sensible and latent heat fluxes

at the air–sea interface for the period 1958–97 were obtained from the National Centers for Environmental Prediction–National Center for Atmospheric Research (the NCEP–NCAR) reanalysis project, a state-of-the-art atmospheric data assimilation system (Kalnay et al. 1996). Surface air temperature is determined prognostically over land and sea ice, and coupled to the sea surface temperature from Reynolds and Smith (1995) over open water. Sea ice coverage, determined from essentially the same observational archives used here (see Kalnay et al. 1996), is specified to be either 0% or 100% in the NCEP–NCAR reanalyses depending on whether the observed values are less than or greater than 55%. The temperature and flux data were provided on a T62 Gaussian grid, and the SLP data on a 2.5° lat × 2.5° long grid. Monthly means were computed from the 6-hourly data.

c. Cyclone frequency

Cyclone counts were obtained from Dr. M. Serreze at the University of Colorado. Following the cyclone detection and tracking algorithms developed in Serreze (1995) and Serreze et al. (1997), storm positions were determined from the 6-hourly NCEP–NCAR reanalysis SLP fields projected onto a 250 km × 250 km equal-area grid. We summed the number of cyclones for each winter (January–March) season during 1958–97 and then smoothed the cyclone totals with a three-point binomial filter in the zonal and meridional directions. We then interpolated the smoothed cyclone counts onto a 1° lat × 1° long grid.

d. Methods

For each year during the period of record common to all the datasets (1958–97), we formed winter (January–March) averages. Anomalies were then computed by subtracting the 40-yr mean from each individual winter. We applied empirical orthogonal function (EOF) analysis to the winter sea ice anomalies to extract the dominant structure of variability. The EOF is based upon the area-weighted covariance matrix. The associated principal component (PC time series) of the EOF was constructed by projecting the anomaly fields for each winter upon the EOF spatial pattern. Thus, the PC is a measure of the degree of similarity between the EOF pattern and the ice anomaly pattern in individual winters. The PC is normalized to unit variance, and the EOF pattern has amplitudes proportional to the percent ice concentration anomaly per unit anomaly of the PC.

Linear regression analysis and compositing were used to determine the anomalies in SLP, cyclone frequency, surface air temperature, and surface energy flux associated with the leading ice PC. Similar measures and techniques were used to diagnose the summer (July–September) sea ice variations.

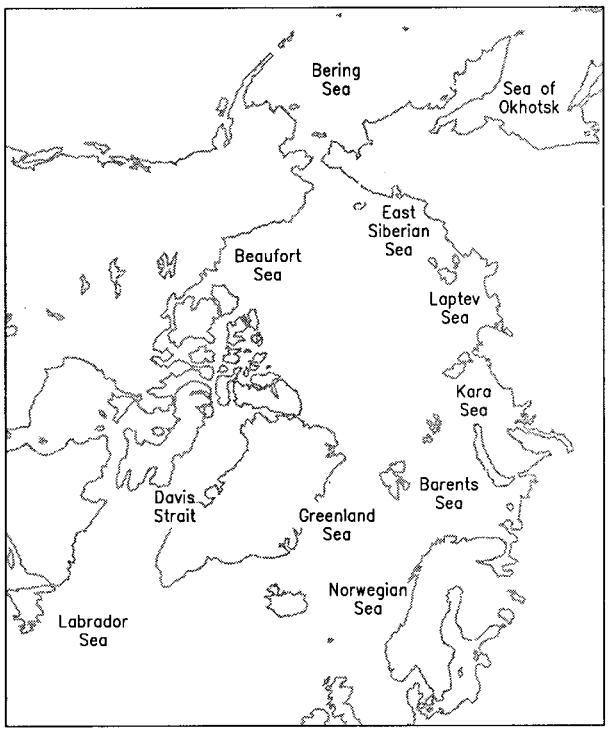

FIG. 1. Map of the Arctic Seas.

3. Results

a. Sea ice variability

The names and locations of the Arctic Seas mentioned in this study are indicated in Fig. 1. The geographical distribution of the standard deviation of winter (January–March) sea ice concentration anomalies during the period 1958–97 is shown in Fig. 2. The climatological marginal ice zone (MIZ), as delineated by the 3% and 97% mean ice concentration isopleths, is also indicated on the figure. The variability is confined to the MIZ, with the largest standard deviations near its center. The variability is greater in the Atlantic sector (values exceeding 25%–30% in the Greenland and Barents Seas and the Davis Strait) than in the Pacific (values exceeding 15%–20% in the Bering Sea and the Sea of Okhotsk). Note that only the northern portion of the Sea of Okhotsk is contained in the Chapman and Walsh (1993) dataset. Similar results are shown in Fang and Wallace (1994) based on a shorter period of record.

The region of maximum variability in the Greenland Sea in Fig. 2 coincides with the sea ice feature known as the ''Odden'' (Shuchman et al. 1998). The Odden is a tongue of sea ice that episodically advances rapidly northeastward into the Greenland Sea from the edge of the main ice pack near 10°W between 72° and 74°N. At least one such advance (and retreat) occurs during most winters; the maximum area of the Odden ranges from close to zero in some winters to nearly 3×10^5 km^2 in other years (Shuchman et al. 1998). The episodic nature

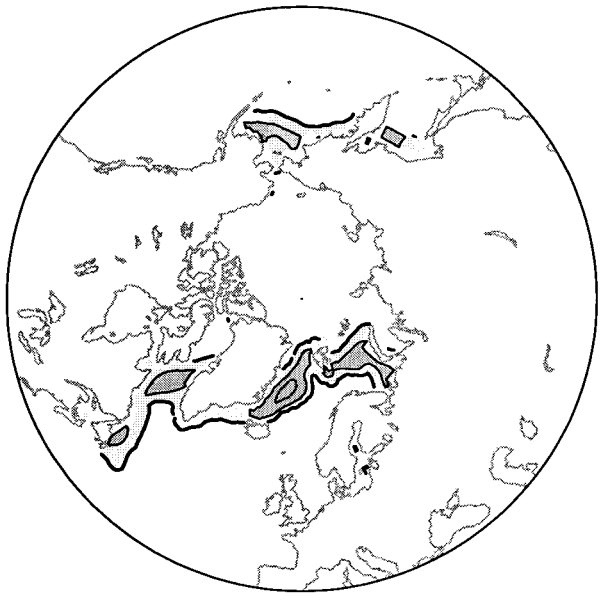

FIG. 2. Standard deviation of January–March ice concentration anomalies during 1958–97 (shading and thin contours). Light shading denotes values between 5% and 15% and dark shading values greater than 15%. The thin solid contour is the 15% isopleth and the thick dashed contour is the 25% isopleth. The thick solid contours denote the 3% and 97% isopleths of the climatological mean winter ice concentration field.

of the Odden is undoubtedly a primary reason why the eastern Greenland Sea contains a variance maximum in Fig. 2.

The leading EOF of winter sea ice concentration anomalies over the Arctic, which accounts for 35% of the variability (compared to 13% for the second model), exhibits largest amplitude in the Atlantic sector, with out-of-phase variations between the Labrador and Greenland–Barents Seas (Fig. 3). A similar but weaker phase opposition is also evident within the Pacific sector between the Bering Sea and the Sea of Okhotsk. The maximum values are 20%–25% (per unit anomaly of the PC) in the Greenland and Barents Seas, and 10%–15% in the Labrador Sea. The out-of-phase behavior of winter sea ice within the Atlantic and Pacific basins is consistent with results from previous studies (e.g., Walsh and Johnson 1979; Rogers and van Loon 1979; Fang and Wallace 1994; Slonosky et al. 1997).

The PC of the leading EOF exhibits low-frequency behavior, with decadal-scale variations superimposed upon a general downward trend (Fig. 3). (Note that negative values of the PC correspond to reduced ice concentrations east of Greenland and increased ice cover west of Greenland.) The high lag-one autocorrelation of the PC (0.69) reflects the predominance of decadal and longer timescale variations. The largest positive anomalies occurred in the late 1960s in association with the Great Salinity Anomaly (Dickson et al. 1988), a period of enhanced wind-driven ice transport from the Arctic through Fram Strait. The maximum negative anomalies

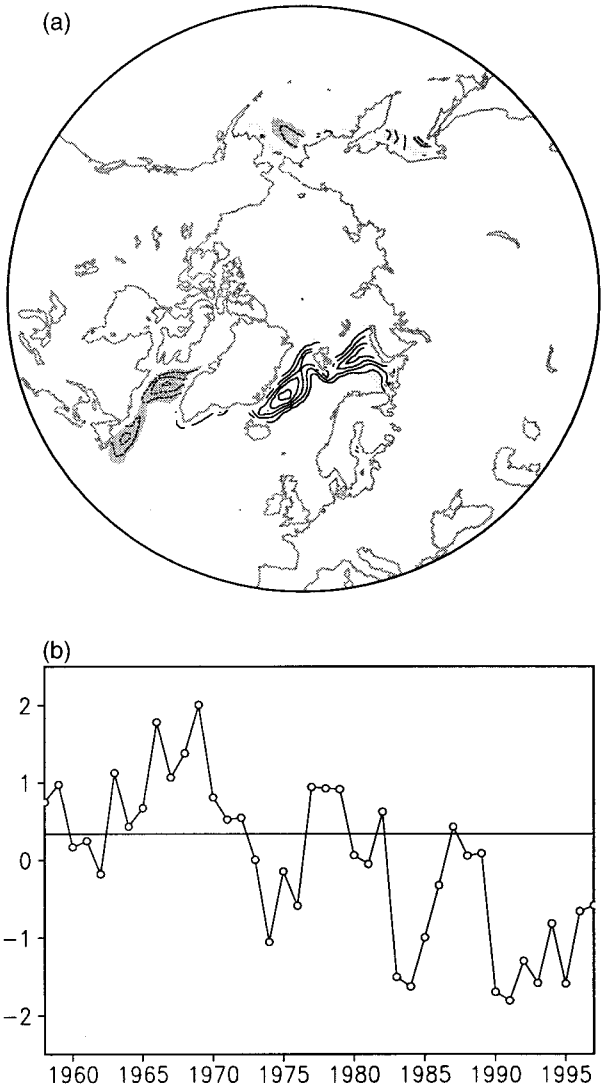

FIG. 3. (a) Leading EOF of winter ice concentration anomalies during 1958–97. The contour interval is 5%, and the zero contour has been omitted. Light (dark) shading denotes values greater than 2% (less than −2%). The EOF accounts for 35% of the variance of winter sea ice over the Arctic. (b) Principal component time series of the leading ice EOF.

occurred during the early 1990s. Thus the temporal trend over the past several decades has been toward less ice in the eastern North Atlantic and more ice in the western North Atlantic. A similar PC was presented in Slonosky et al. (1997) based on the period 1954–90, although it accounted for a lower fraction of the total variance (23%) than that found here. The east–west contrast in the trends over the North Atlantic is also clearly apparent in Parkinson et al.'s (1999) analysis of sea ice data for the post-1978 period.

As in the case of the total variance (Fig. 2), the EOF loadings of Fig. 3 contain a maximum in the Greenland Sea where the Odden feature occurs. The temporal variations of EOF 1 indeed correspond well with the annual

time series of Odden mean sea ice area for 1979–94 as compiled from satellite passive microwave data by Shuchman et al. (1998). The correlation between the Odden time series and PC1 (Fig. 3) during this 16-yr period is 0.64, which is surprisingly large considering that EOF1 describes the variations of the sea ice margin throughout the Northern Hemisphere. The implication is that the atmospheric factors controlling the variability of the Odden (see Shuchman et al. 1998) covary with a larger-scale atmospheric circulation pattern that affects sea ice hemispherically. The associated hemispheric-scale atmospheric variability is addressed in the following sections.

b. Relation between sea ice and sea level pressure

The SLP anomaly field associated with the leading EOF of sea ice was determined from a linear regression of the winter SLP anomalies at each grid point upon the ice PC time series. The regression coefficients are in units of mb per standard deviation of the ice PC. To assign more convenient and physically meaningful units to the regression field, we multiplied the regression coefficients by -2.3, the value of the 40-yr linear trend in the ice PC. Thus, the resulting regression field is representative of the SLP anomaly associated with the 40-yr trend in the ice PC. A composite of SLP anomalies based upon extreme years in the ice PC record yields a pattern that is nearly identical to that obtained from the regression procedure but with slightly larger amplitude, as we shall show in section 3e.

The SLP anomaly pattern that accompanies the leading EOF of Arctic sea ice (Fig. 4) exhibits below-normal values over the Arctic, with maximum negative anomalies [-8 to -9 mb (40 yr)$^{-1}$] directly east of Greenland, and above normal values [4–6 mb (40 yr)$^{-1}$] along 40°N over the eastern Atlantic extending into Europe. Weaker SLP anomalies [± 2 mb (40 yr)$^{-1}$] are found over the North Pacific and Kamchatka. This pattern (excluding the North Pacific sector) is strongly reminiscent of the positive polarity of the NAO (Hurrell 1995) and AO (Thompson and Wallace 1998), although the details of the pattern east of Greenland are distinctive (see section 3e). The Aleutian lobe in Fig. 4 is opposite in sign to the corresponding feature in the AO of Thompson and Wallace.

The SLP pattern shown in Fig. 4 implies anomalous southerly geostrophic winds across the Greenland and Barents Seas and anomalous north-northwesterly flow in the Labrador Sea when the ice PC is below normal. Such wind variations are qualitatively consistent with the notion that the sea ice anomalies are directly forced by the atmosphere, either thermodynamically through advected surface air temperature anomalies or dynamically through wind-driven ice drift anomalies. For example, anomalous advection of warm air from the south over the Greenland and Barents Seas will promote ice-melt and as well a dynamic retreat of the ice edge.

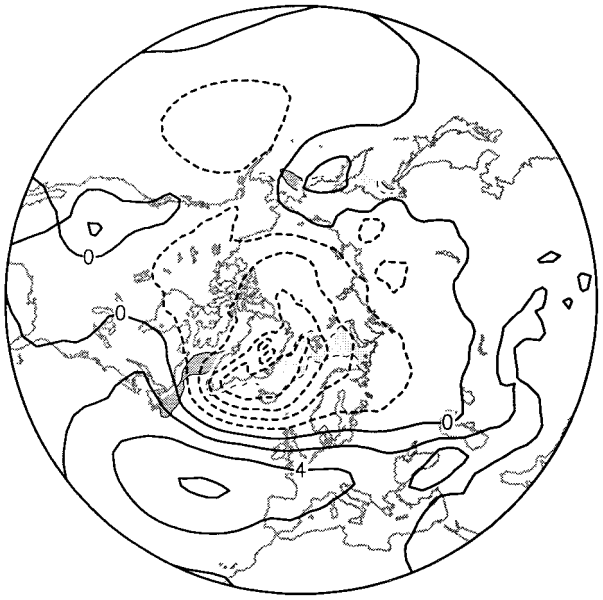

FIG. 4. Winter SLP (contours) and ice concentration (shading) anomalies associated with the leading ice EOF. The patterns were constructed by linearly regressing the SLP and ice anomalies upon the ice PC and multiplying the regression coefficients by -2.3, the value of the 40-yr linear trend in the ice PC. The SLP anomaly field is in units of mb (40 yr)$^{-1}$, contoured every two units. Light (dark) shading denotes ice concentration anomalies greater than 8% (40 yr)$^{-1}$ [less than -8% (40 yr)$^{-1}$].

Analogous arguments can be made for the Labrador Sea and for the weaker SLP–ice anomalies in the Pacific sector. Indeed, a comprehensive sea ice model forced with observed geostrophic surface winds during 1946–93 obtains a qualitatively similar pattern of sea ice anomalies (S. Hakkinen 1998, personal communication). Similar relationships between wintertime SLP and sea ice anomaly fields have been documented by Rogers and van Loon (1979), Fang and Wallace (1994), Mysak et al. (1996), and Slonosky et al. (1997), among others.

Further support for the notion that the atmospheric circulation controls the sea ice anomaly pattern depicted in Fig. 4 comes from lead–lag relationships between the ice PC and SLP. Figure 4 contains an implicit 2-week lead between the SLP and ice fields since the SLP data are centered at the midpoint of the month while the sea ice data are reported at the end of the month. A simple index of the magnitude of the SLP pattern shown in Fig. 4 is the difference between the maximum value near 40°N and the minimum value over the Greenland Sea (15 mb). For comparison, the December–February (February–April) SLP index value is 15.5 mb (8.6 mb). Thus, the implied wind forcing of the sea ice field is substantially stronger when SLP leads the ice by 2–6 weeks than when it lags the ice by 2 weeks. This result is consistent with the findings of Fang and Wallace (1994). The temporal correlation coefficient between the time series of the SLP pattern shown in Fig. 4 (obtained by projecting the SLP regression pattern poleward of

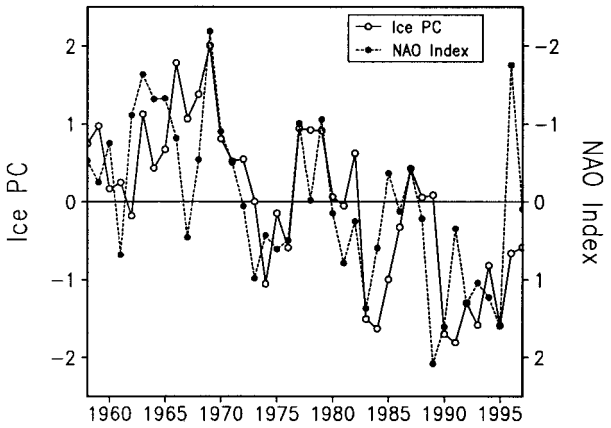

FIG. 5. Winter NAO index and the ice PC. Units are standard deviations. Note that the scale for the NAO index has been inverted.

35°N onto the SLP anomaly field each winter) and the ice PC is 0.63 (0.61 for February–April and 0.73 for December–February).

As mentioned above, the pressure pattern shown in Fig. 4 is reminiscent of the NAO. Figure 5 shows the NAO record (defined as the December–March normalized SLP difference between Lisbon, Portugal, and Stykkisholmur, Iceland) superimposed upon the ice PC index (note that the NAO scale has been inverted). The two time series are broadly similar (their linear correlation coefficient is 0.63), but individual winters can be radically different. For example, the (inverted) NAO index was low in both 1989 and 1990, yet the ice PC was near normal in 1989 and low in 1990. Figure 6 shows that the January–March SLP anomalies in 1989 were nearly uniform from Iceland to the central Arctic, while in 1990 they were amplified near Iceland (very similar patterns obtain for December–February, not shown). Thus, the implied geostrophic meridional wind pattern across the Greenland and Barents Seas was very different in the two winters, with strong southerly wind anomalies favoring ice retreat as observed in 1990, and negligible meridional wind anomalies consistent with the near-normal ice conditions in 1989. Other years in which the NAO was extreme but the ice PC was near normal (e.g., 1961, 1973, and 1985) exhibit a similar lack of geostrophic meridional wind component east of Greenland (not shown). Thus, a simple index such as the NAO, while a useful indicator of the large-scale atmospheric circulation, may be inadequate for inferring the details of atmospheric forcing relevant for the sea ice margin.

c. Relation between sea ice and surface air temperature

The linear regression pattern of SAT upon the ice PC record is shown in Fig. 7. Since SAT variations are considerably smaller over the oceans than over land, we have included the ± 0.5°C (40 yr)$^{-1}$ contour over ocean

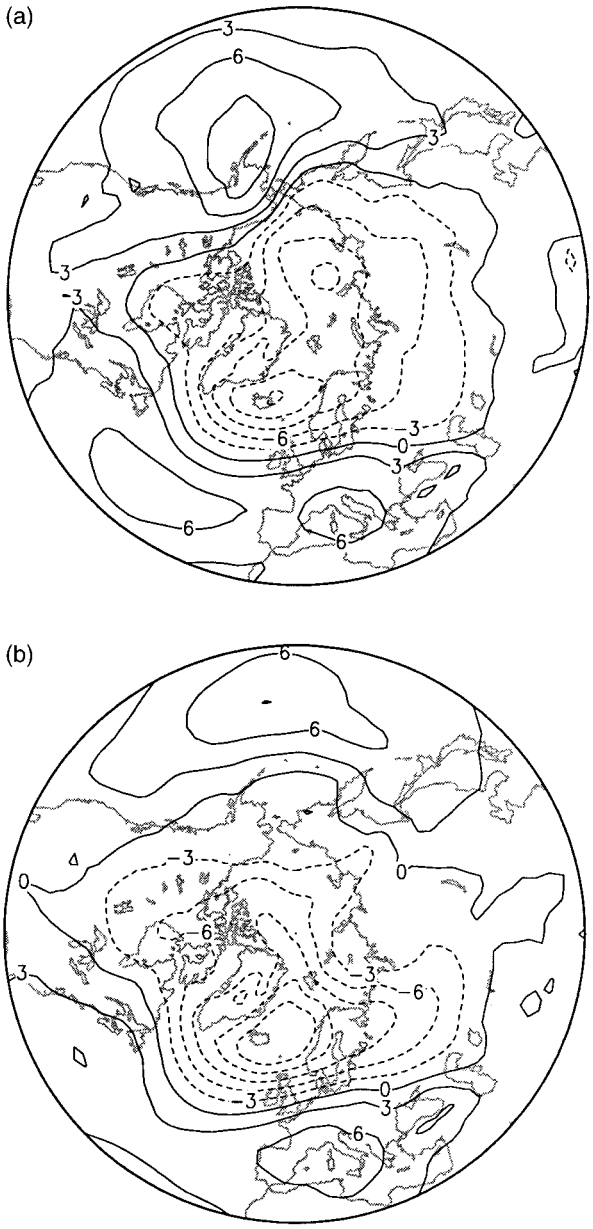

FIG. 6. Winter SLP anomalies (mb) for (a) 1989 and (b) 1990. The contour interval is 3 mb and negative contours are dashed.

areas only. As with SLP, the large-scale pattern of SAT anomalies associated with the leading EOF of sea ice is similar to that accompanying the NAO (Hurrell and van Loon 1997) and AO (Thompson et al. 2000): positive anomalies over northern Eurasia and northwestern Canada, and negative anomalies over northeastern Canada and Greenland, with values as large as 2°–3°C (40 yr)$^{-1}$ over the land surface. The largest SAT changes [approximately 10°C (40 yr)$^{-1}$] occur over the sea ice anomalies, with warming coincident with the reduced ice cover in the Greenland and Barents Seas and cooling over the increased ice amounts in the Davis Strait. Am-

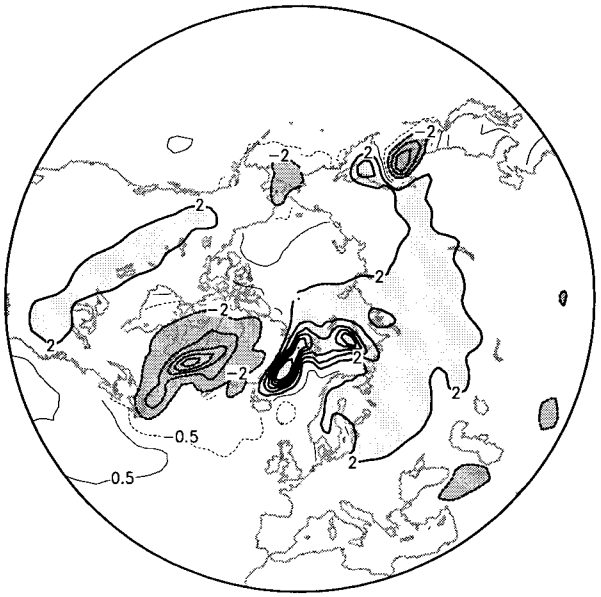

FIG. 7. As in Fig. 4 but for surface air temperature. The contour interval is 2°C (40 yr)$^{-1}$ and the zero contour is omitted. Light (dark) shading denotes temperature anomalies greater than 2°C (40 yr)$^{-1}$ [less than −2°C (40 yr)$^{-1}$]. The ±0.5°C contours are included over ocean areas only.

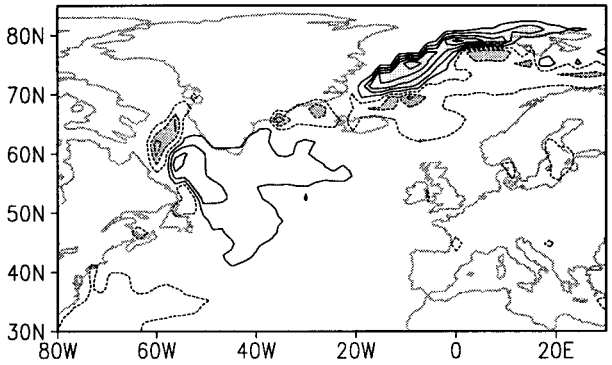

FIG. 8. As in Fig. 4 but for upward surface latent-plus-sensible heat flux over the Atlantic sector. The contour interval is 50 W m^{-2} (40 yr)$^{-1}$ starting at ±25 W m^{-2} (40 yr)$^{-1}$. Light (dark) shading denotes heat flux anomalies greater than 75 W m^{-2} (40 yr)$^{-1}$ [less than −75 W m^{-2} (40 yr)$^{-1}$].

plified SAT anomalies also occur over the sea ice perturbations in the Pacific sector. [Note that the station-based SAT dataset used in the studies of Hurrell and van Loon (1997) and Thompson et al. (1999) does not contain any information over sea ice.]

The broad-scale pattern of temperature anomalies in Fig. 7 is consistent with advection by the large-scale atmospheric circulation (see also Thompson et al. 2000), while the more localized SAT anomalies over sea ice may be attributed to the sea ice anomalies themselves. Although large changes in SAT over ice cover anomalies are to be expected due to the strong contrast between sea surface and ice surface temperatures, the changes in Fig. 7 may be exaggerated because of the crude binary representation of the marginal ice zone in the NCEP–NCAR reanalyses (sea ice concentrations are specified to be either 0% or 100%). The marginal ice zone is, in reality, a mixture of ice types and surfaces; total ice concentrations range from essentially zero to unity. Results from field programs such as Surface Heat Budget of the Arctic Ocean (SHEBA) (Moritz et al. 1993) should provide a more realistic assessment of the SAT changes associated with changes in ice concentration.

d. Relation between sea ice and surface latent and sensible heat flux

Changes in sea ice concentration can affect the atmospheric circulation through changes in surface albedo and surface fluxes of heat, moisture, and momentum. In winter, the albedo effect is supressed due to the low insolation. The linear regression pattern of surface turbulent (sensible + latent) heat flux anomalies upon the ice PC record is shown in Fig. 8 for the Atlantic sector. Positive values indicate above-normal heat transfer from the ocean to the atmosphere when the ice PC index is below normal. The largest heat flux changes occur near the ice edge, where they are nearly an order of magnitude larger than those over the open ocean (250 W m^{-2} as opposed to 25 W m^{-2}). In particular, positive upward heat flux anomalies are associated with reduced ice cover in the Greenland/Barents Seas, and negative upward heat flux anomalies with enhanced ice concentration in the Labrador Sea. The maximum flux anomalies exceed 250 W m^{-2} (40 yr)$^{-1}$ in the Greenland Sea. For comparison, we note that the mean upward heat flux over the Gulf Stream in winter is 350–400 W m^{-2}.

The large heat flux anomalies over the MIZ are accompanied by anomalies of opposite sign equatorward of the ice edge. We interpret this dipole pattern to be the result of the atmospheric circulation anomalies responsible for the ice cover changes. For example, in the case of strong northerly wind anomalies over the Greenland and Barents Seas, the ice edge advances, reducing the ocean-to-atmosphere heat flux locally but enhancing it on the equatorward side of the ice boundary due to the flow of abnormally cold air over the relatively warm ocean surface. A similar dipole pattern has been found in general circulation model experiments with perturbed sea ice concentrations (Simmonds and Budd 1991).

The surface flux anomalies in Fig. 8 are reanalysis derived and hence are dependent on the NCEP–NCAR model parameterizations. As with the SAT fields, the surface heat flux anomalies associated with changes in ice cover may be overestimated in the NCEP–NCAR reanalyses, primarily because of the binary representation of ice coverage. However, the amplification of the heat flux changes over ice relative to open ocean is undoubtedly correct in a qualitative sense because even a partial ice cover reduces substantially the surface–

atmosphere exchanges of heat and moisture by virtue of the strong contrast between ice surface and sea surface temperatures.

e. Relation between sea ice and cyclone counts

The large heat flux perturbations associated with changes in sea ice cover suggest that the atmospheric circulation may be sensitive to the observed sea ice variations in the Atlantic sector, particularly in the active stormtrack region east of Greenland. It is worth noting that the heat flux anomalies due to ice cover changes (200–250 W m^{-2}) are approximately an order of magnitude larger than those induced by midlatitude SST variations. In particular, a 0.5°C SST anomaly (typical of the extratropics in winter; recall Fig. 7) would produce an upward turbulent heat flux anomaly of less than 20 W m^{-2} according to the standard bulk formulas (cf. Hsiung 1986).

To investigate whether the changes in surface turbulent heat flux induced by variations in sea ice coverage have any impact upon cyclone frequencies, we composited storm counts for the winters in which the ice PC index exceeds one standard deviation (1963, 1966, 1967, 1968, 1969) and for the winters in which the ice PC index is less than minus one standard deviation (1974, 1983, 1984, 1990, 1991, 1992, 1993, 1995). Recall that the storm positions are identified according to the location of low pressure centers at sea level (section 2c). We also composited the ice concentration values according to the same criteria. The high and low composites and their difference are shown in Fig. 9 for the subpolar North Atlantic.

In the high ice composite (Fig. 9a), the ice edge east of Greenland extends from northern Iceland to Svalbard to the southern tip of Novaya Zemlya. The stormtrack reflects the position of the sea ice boundary, with the northern portion of the four storm count isopleth approximately coincident with the 60% ice concentration isopleth. In the low ice composite (Fig. 9b), the ice edge east of Greenland is retracted poleward and the stormtrack expanded northwestward into the Greenland Sea relative to the high ice composite (note again the correspondence between the four storm count isopleth and the 60% ice concentration isopleth, both of which are farther to the northwest in Fig. 9b than in Fig. 9a). The low-minus-high composite difference field (Fig. 9c) exhibits an increase in cyclone numbers between Greenland and Iceland in the region of the climatological mean Icelandic low and directly east of Greenland where the sea ice concentrations have decreased.

We hypothesize that the increase in storm counts directly over the reduced sea ice coverage in the Greenland Sea is a result of the ice-induced variations in the surface energy flux into the atmosphere from the lower boundary. We note that the proximity of the stormtrack to the ice edge east of Greenland may enhance the sensitivity of cyclone activity in this region to changes in sea ice extent. Indeed, the low-level baroclinicity associated with the mean ice–ocean boundary has been shown to influence the formation of polar lows in the Greenland Sea, both in observations (Carleton 1985a,b; Rasmussen 1985) and in model simulations (Sardie and Warner 1985). Thus, changes in Greenland Sea ice cover induced by large-scale atmospheric circulation anomalies may feed back upon the atmosphere by altering cyclone activity locally over the MIZ. We also note the possibility that the increase in cyclone counts over the Greenland Sea in winters of reduced ice cover may result from the interaction of the anomalous large-scale atmospheric flow with the orography over Greenland.

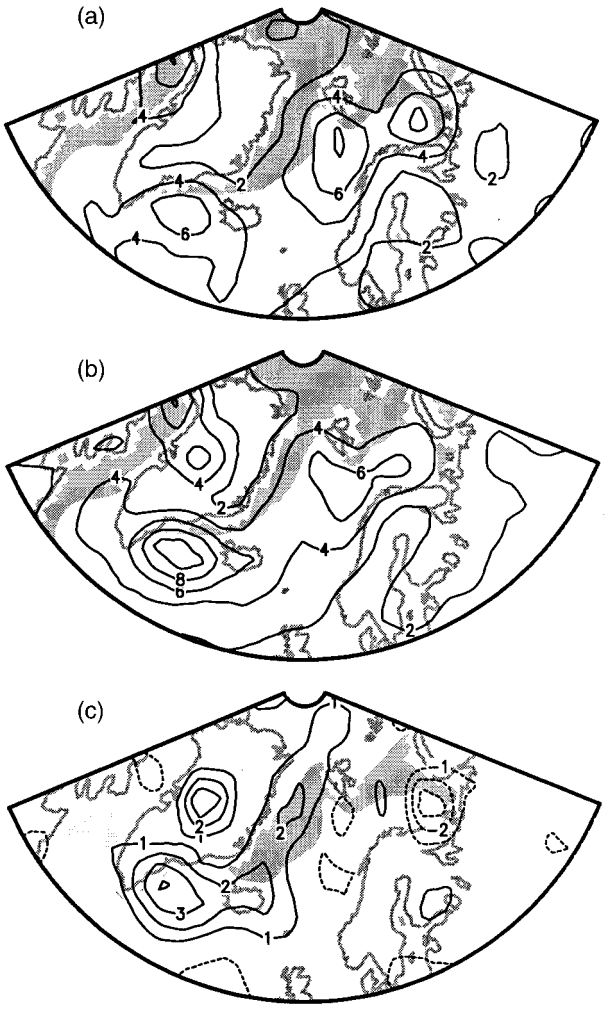

FIG. 9. Composites of winter cyclone counts (contours) and sea ice concentrations exceeding 60% (shading) for winters with (a) high and (b) low values of the ice PC. (c) Low-minus-high composite differences. The cyclone counts represent the number of storms per 250 km × 250 km area per winter season. The contour interval for the storm count difference field is 1, with the zero contour omitted. Light (dark) shading denotes ice concentration differences greater than 20% (less than −20%). Cyclone count differences greater than one are statistically significant at the 95% confidence level according to a Student's t-test.

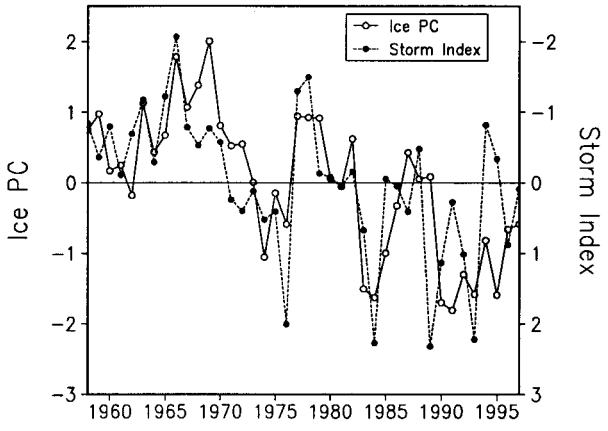

FIG. 10. Regional index of cyclone counts over the Greenland Sea and the ice PC. Units are standard deviations. Note that the scale for the cyclone index has been inverted.

The time series of the number of cyclones per winter season in the area directly east of Greenland and north of Iceland (delineated by the +1 contour in the bottom panel of Fig. 9) is shown together with the ice PC index in Fig. 10. Note that the cyclone scale has been inverted. The correspondence between the two records is quite good on the decadal timescale: their linear correlation coefficient is 0.65 (0.85 if a 3-yr running mean is applied). However, the (inverted) cyclone index does not remain as low as the ice PC during the 1990s.

The NAO plays a major role in the variability of North Atlantic cyclone activity (Rogers 1990; Serreze et al. 1997). Are the cyclone frequency changes that occur near the ice edge over the Greenland Sea unique to composites keyed to the ice PC, or do they also occur in composites based upon the NAO index? Figure 11 shows the composite differences of SLP and cyclone frequency based upon the ice PC index (left) and the NAO index (right). The high NAO composite is based upon the winters for which the NAO index exceeds one standard deviation (1983, 1989, 1990, 1992, 1993, 1994, 1995). Similarily, the low NAO composite is based upon the winters for which the NAO index is less than minus one standard deviation (1962, 1963, 1964, 1965, 1969, 1977, 1979, 1996). Note that the high NAO and low ice PC composites contain two years in common and the low NAO and high ice PC composites contain five years in common. The statistical signficance of the low-minus-high composite differences was assessed according to a local Student's t-test. As a rough guide, cyclone differences exceeding unity and SLP differences less than −8 mb are significant at the 95% level for the domain shown in Fig. 11.

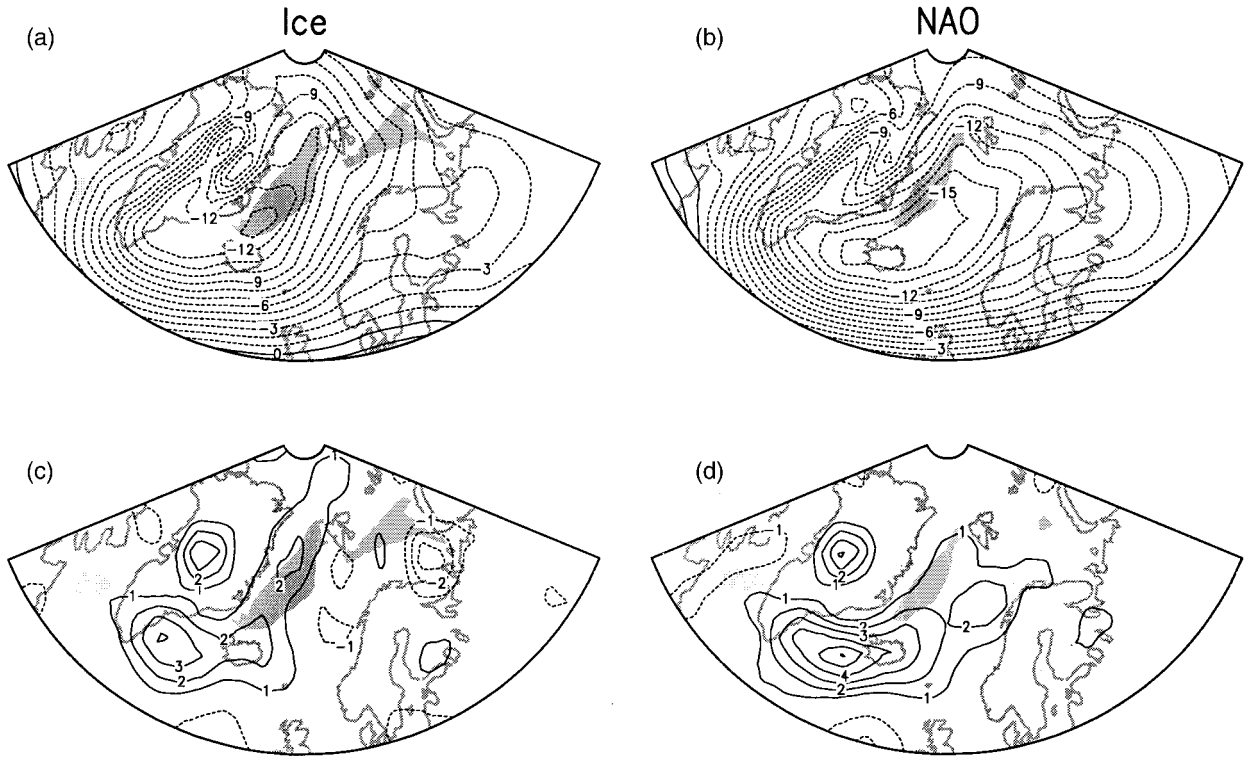

FIG. 11. (Left) Low-minus-high composite differences of winter (a) SLP (mb) and (c) cyclone counts based upon the ice PC record. (Right) High-minus-low composite differences of winter (b) SLP (mb) and (d) cyclone counts based upon the NAO index. The shading in all four panels denotes the corresponding composite differences of sea ice concentration (light shading for values greater than 35% and dark shading for values less than −35%).

The composite differences based upon the ice PC index (Fig. 11, left) exhibit a local minimum in SLP and a local maximum in cyclone frequency directly over the reduced sea ice concentrations in the Greenland Sea–Fram Strait corridor. In constrast, the belt of lowest pressure and highest cyclone counts in the NAO-based composite differences (Fig. 11, right) are not confined to the region of reduced ice cover (which is much less pronounced than in the ice PC composite), but occur south of the ice edge where the mean stormtrack and Icelandic low are located. It may be noted that the cyclone frequency differences over the Norwegian and Barents Seas are of opposite polarity in the NAO and ice-based composites.

Many earlier studies, ranging from Wiese (1924) to Mysak and Power (1992), have hypothesized that reduced sea ice coverage should contribute to changes in cyclone activity. The results in Figs. 9–11 suggest that cyclone frequency (and mean SLP) may respond to sea ice and that the response is not simply a reflection of the large-scale circulation variability associated with the NAO. We note that the local decrease in SLP over the reduced ice amounts in the Greenland Sea in the ice PC composite difference (Fig. 11a) is qualitatively consistent with the results of idealized atmospheric general circulation experiments in which a prescribed sea ice margin is altered artificially (Herman and Johnson 1978; Simmonds and Budd 1991; Rind et al. 1995).

f. Summer sea ice variability

As discussed in the introduction, summer Arctic sea ice extent has been diminishing at a rate of 4%–6% decade^{-1}, both for the most recent period (1979–95; Cavalieri et al. 1997; Parkinson et al. 1999; Maslanik et al. 1996) and for previous decades (1961–91; Chapman and Walsh 1993). How are the sea ice trends in summer related to those in winter? Do atmospheric circulation anomalies play a role in forcing the summer ice variations?

Although an analysis of the full record (1957–96) of summer sea ice concentrations is desirable, the pronounced downward discontinuity from 1978 to 1979 (due to the introduction of satellite passive microwave sensing techniques that depict lower summer ice concentrations within the pack ice) precludes such an analysis with the present dataset (see Fig. A1 in the appendix for the summer Arctic ice concentration record). However, the record of summer ice *extent* as opposed to concentration appears to be less sensitive to the changes in remote sensing techniques, presumably because the occurence of open water with the pack ice occurs preferentially at relatively high ice concentrations (higher than 15%, which is the conventional definition used for ice extent). Thus, we rely on ice extent as our primary variable for studying the long-term summer variability, although we also show results based upon ice concentration for the two subperiods 1957–78 and 1979–96.

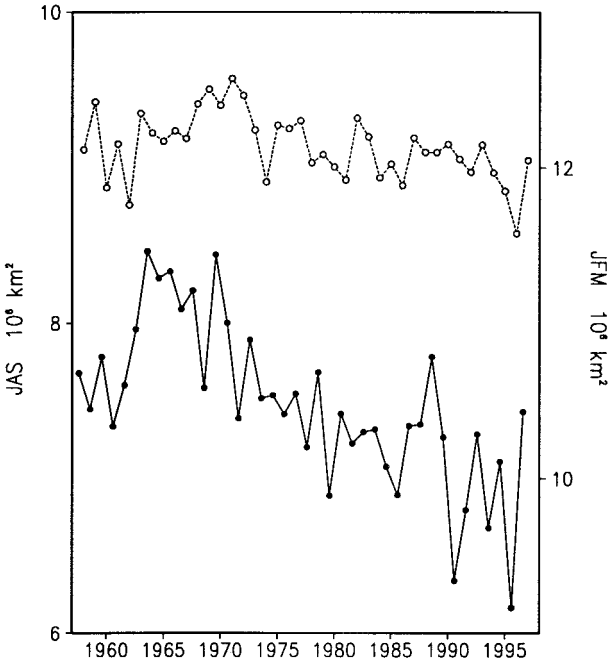

FIG. 12. Time series of Arctic sea ice extent averaged over the polar cap in winter (dashed curve) and summer (solid curve). Note the different scales for winter and summer. Units are 10^6 km^2.

The merging of the passive microwave ice concentration measurements with earlier data sources during the melt season remains an important topic for future research.

Figure 12 shows the winter (1958–97) and summer (1957–96) sea ice extent records for the Arctic as a whole, where ice extent is defined according to the position of the 15% ice concentration boundary. The linear trend in summer Arctic ice extent during 1957–96 is -0.30×10^6 km^2 decade^{-1} or -4.0% decade^{-1} relative to the mean, comparable to the results shown in Chapman and Walsh (1993) based upon the period 1961–90 (-3.6% decade^{-1}). In winter, the linear trend is small: -0.08×10^6 km^2 or -0.6% decade^{-1}, also in agreement with Chapman and Walsh. On a regional basis, however, the trends in winter are just as large as those in summer (Fig. 13). In winter, the positive trends in the Labrador Sea offset the negative trends elsewhere to produce near-zero change in the zonal average.

The summer Arctic ice extent record is nearly identical to the leading principal component of the summer ice extent field (not shown), which accounts for 31% of the variance: the correlation coefficient between the two time series is 0.98. Similarly, the spatial pattern of the leading EOF of summer ice extent (not shown) resembles closely the pattern of linear trends in Fig. 13.

It is instructive to compare the dominant pattern of sea ice variability in winter with that in summer. Both seasons contain long-term trends during the past 40 yr (Figs. 3 and 12). However, in summer the trend is relatively monotonic, while in winter it is superimposed

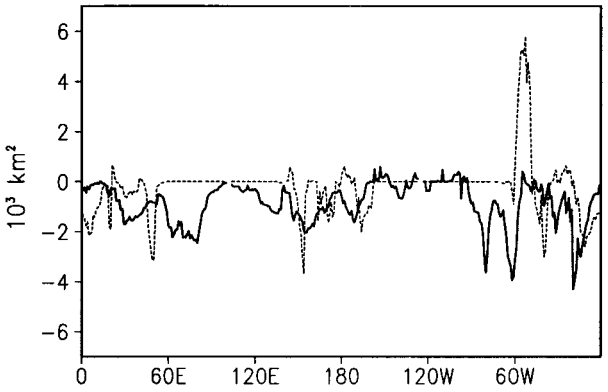

FIG. 13. Linear trends in sea ice extent as a function of longitude based on the period 1958–97 for winter (dashed curve) and 1957–96 for summer (solid curve). Units are 10^3 km^2 decade^{-1}.

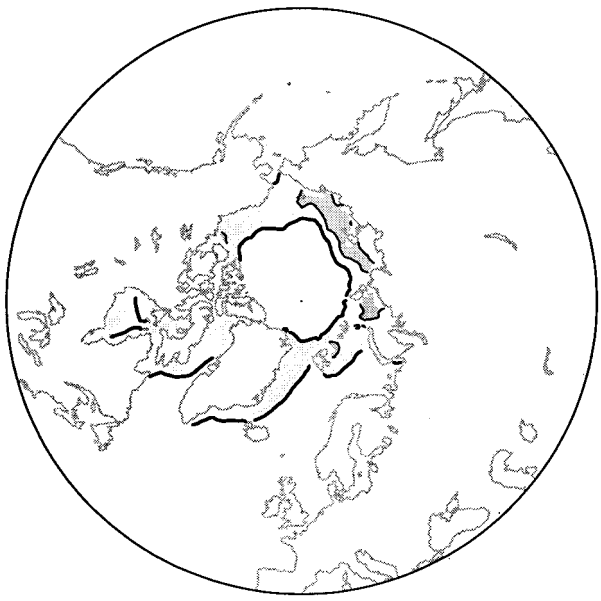

FIG. 14. Standard deviation of July–September ice concentration anomalies during 1957–91 (shading and thin contours). Light shading denotes values between 5% and 15% and dark shading values greater than 15%. The thin solid contour is the 15% isopleth and the thick dashed contour is the 25% isopleth. The thick solid contours denote the 3% and 97% isopleths of the climatological mean summer ice concentration field. For this figure only, the summer sea ice concentrations are based upon a dataset that does not include the discontinuity in 1979 associated with the introduction of satellite passive microwave data (W. Chapman 1998, personal communication). Standard deviation maps for the early (1957–78) and later (1979–96) portions of the record (the latter containing passive microwave data) look qualitatively similar (not shown).

upon decadal-scale fluctuations. The temporal correlation coefficient between the leading winter and summer ice PC records is 0.74 for winter leading summer by 6 months (0.63 for summer leading winter by 6 months), reflecting that the downward trend is common to both time series. The spatial patterns of sea ice variability also differ between the seasons. The winter pattern (Fig. 3) consists of regional anomalies of opposing sign that largely cancel in the zonal average, while the summer pattern (Fig. 13) is more zonally uniform. The spatial and temporal differences between winter and summer variability in Arctic sea ice are reminiscent of those in Northern Hemisphere air temperature documented by Wallace et al. (1993, 1996). These authors argue that the thermal variations in summer are radiatively forced while those in winter contain both radiative and ''circulation-induced'' components.

The mean and standard deviation of the summer (July–September) sea ice concentration field is shown in Fig. 14. Compared to winter, the summer ice pack is contracted poleward with much of the MIZ located north of 75°N. As in winter, the variability is confined to the MIZ, with maximum values (15%–20%) in the Siberian sector.

The spatial distributions of the linear trends in summer ice concentration during 1957–78 and 1979–96 are shown in Fig. 15. The average of the trends in the two subperiods is also shown; these provide an estimate of the total summer ice concentration trends during 1957–96. Decreases in sea ice concentration [5%–30% decade^{-1}] are evident during both periods, but the spatial patterns are slightly different. In the earlier period, negative trends extend from Greenland eastward to the date line, with the largest values in the Barents, Kara, and Laptev Seas (20°–135°E). In the later period, the negative trend is focused largely in the east Siberian Sea. The trends for the later period are consistent with those shown in Parkinson et al. (1999).

The time series of summer ice extent for the Barents–Kara–Laptev Sea region (20°–135°E) and the east Siberian Sea (135°E–180°) are shown in Fig. 16. Summer ice extent in the Barents–Kara–Laptev Sea sector is high during the 1960s, with relatively stable conditions since (apart from the large negative anomaly in 1995). In contrast, summer ice extent in the east Siberian Sea is relatively stable during the 1960s–1980s followed by a period of low ice cover during 1989–95 [note that the values during 1957–62 in the Siberian sector likely suffer from a shortage of data; Chapman and Walsh (1993)]. These results are consistent with the ice concentration trend maps shown in Fig. 15.

g. Relation of summer sea ice trends to the atmospheric circulation

Has the atmospheric circulation played a role in reducing the summertime Arctic sea ice extent, or are the summer ice declines a reflection of the general warming trend over the Northern Hemisphere during the past 30–40 yr? To investigate this question, we have regressed the late spring (April–June) SLP anomaly field (other seasons are examined below) upon an index of summer sea ice extent. In view of the differences in the spatial

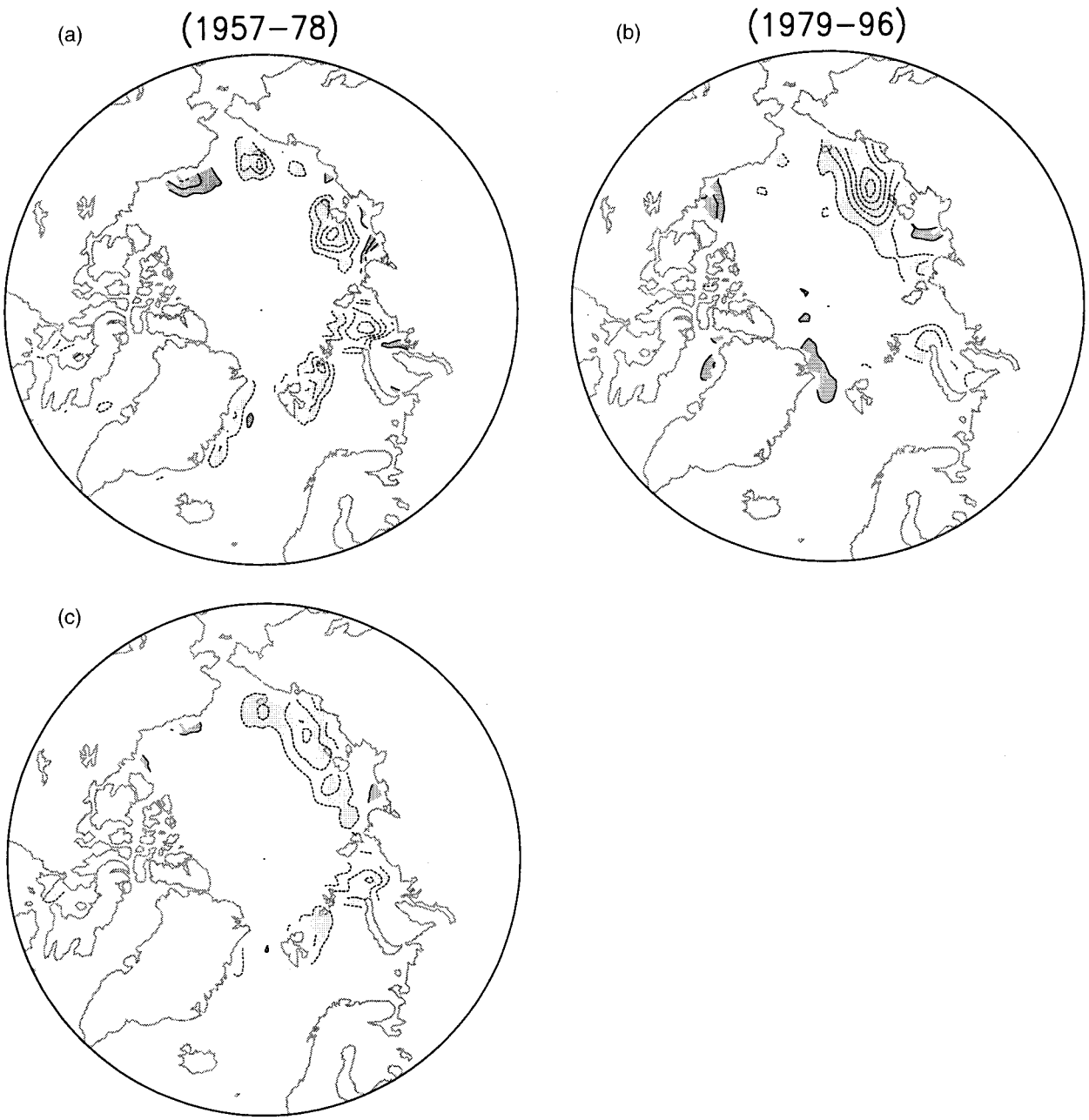

FIG. 15. Linear trends in summer sea ice concentration during (a) 1957–78, (b) 1979–96, and (c) their average. Light (dark) shading denotes values less than −5% decade^{-1} (greater than 5% decade^{-1}). The contour interval is 5% decade^{-1}, and the zero contour has been omitted.

patterns of ice retreat during 1958–78 and 1979–96 (recall Fig. 15), we have performed a separate regression analysis for each subperiod. For the early years, we have used the record of summer ice extent averaged from 20° to 134°E as our ice index, while for the later period we have used ice extent averaged from 135°E to 180°. Both indices reflect the region of largest sea ice declines during the period for which they are defined (recall Fig. 15).

The spring SLP regression map for 1958–78 (Fig. 17a) exhibits positive values centered over the high Arctic (poleward of approximately 70°N) and over the North Atlantic west of the United Kingdom (note that the SLP regression coefficients have been multiplied by −1 to correspond to a negative unit departure of the normalized sea ice index). Thus, when summer ice extent is below normal across the Barents, Kara, and Laptev Seas, spring SLP is above normal over the high

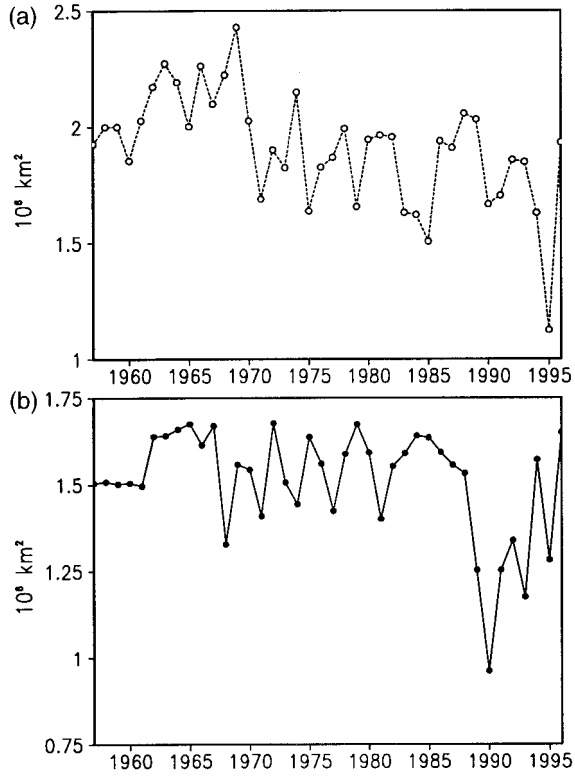

FIG. 16. Time series of summer ice extent in (a) the Barents–Kara–Laptev Sea region (20°–35°E) and (b) the east Siberian Sea (135°E–180°). Units are 10^6 km^2.

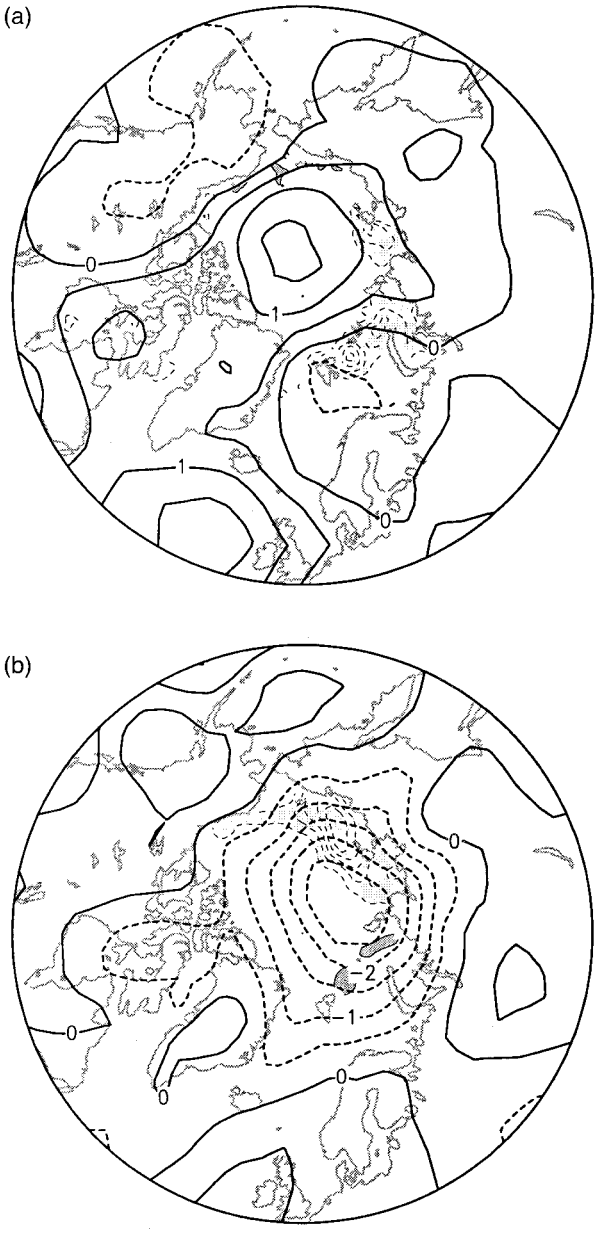

FIG. 17. (a) Regression map of spring (April–June) SLP (thick contours) and summer (July–September) sea ice concentration (shading and thin contours) anomalies based upon the record of summer ice extent in the region (20°–135°E) during the period 1958–78. Both the SLP and ice regression fields have been multiplied by −1. Units are mb for SLP (ice concentration). Light (dark) shading denotes ice concentration values less than −5% (greater than 5%) per unit standard deviation of the ice extent index. The contour interval is 5% per decade, and the zero contour has been omitted. (b) As in (a), but based on summer ice extent in the region (135°E–180°) during the period 1979–96.

Arctic and North Atlantic, and below normal in surrounding regions. This SLP regression pattern is indicative of an anomalous southerly wind component over the region of below-normal summer sea ice concentrations (see Fig. 17). The spring SLP regression map for 1979–96 (Fig. 17, bottom panel) exhibits negative values over the high Arctic and positive values over much of the surrounding area. Thus, when summer ice extent is below normal in the east Siberian Sea, spring SLP is below normal in the high Arctic and above normal to the south. The SLP regression pattern is indicative of an anomalous southerly wind component over the region of reduced summer sea ice concentrations in the east Siberian Sea, and an anomalous northerly wind component over the area of increased sea ice in the Barents and Kara Seas (see Fig. 17). It should be noted that the SLP regression maps for the two subperiods differ considerably, particularly over the high Arctic where the values are of opposite sign. Nevertheless, both SLP patterns are physically consistent with the notion that spring atmospheric circulation anomalies were instrumental in forcing the observed summer sea ice changes.

To give an indication of how strongly coupled the SLP patterns depicted in Fig. 17 are to the sea ice indices upon which they were based, we show the time series of the sea ice index with its associated SLP pattern index, defined by projecting the SLP regression pattern poleward of 70°N upon the SLP anomaly field in each spring (Fig. 18). The temporal correspondence between the regional summer sea ice indices and their associated

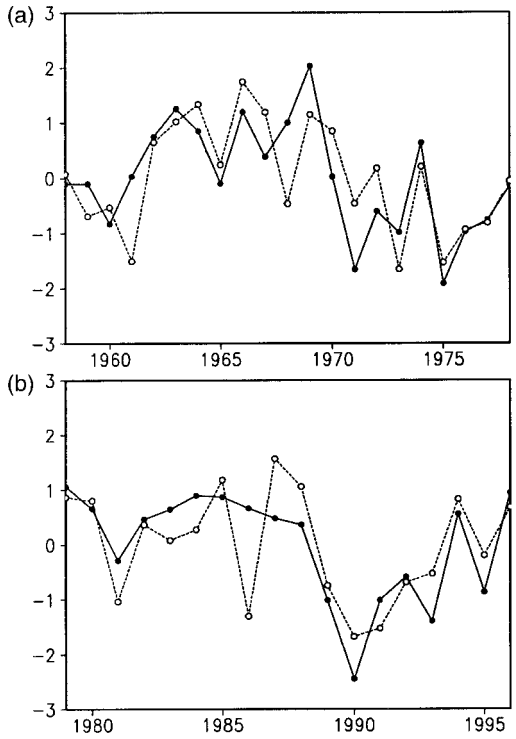

FIG. 18. (a) Time series of normalized summer ice extent in the Barents–Kara–Laptev Sea region (20°–135°E; solid curve) and the associated spring SLP anomaly pattern index (dashed curve; see text for details). (b) Time series of normalized summer ice extent in the east Siberian Sea (135°E–180°; solid curve) and the associated spring SLP anomaly pattern index (dashed curve).

spring SLP pattern indices is remarkable: the correlation coefficient between each sea ice–SLP pair is 0.73.

We have also performed regression analyses between the summer ice extent indices and the SLP anomaly fields during early summer (May–July) and high summer (June–August). For the period 1958–78, the correlation coefficient between the summer sea ice index and the time series of the projection of the SLP regression pattern poleward of 70°N is weaker in May–July (0.65) and June–August (0.55) than in April–June (0.73). For the period 1979–96, the correlation coefficient is slightly stronger in May–July (0.76) than in April–June (0.73), and weaker in July–August (0.58). On the basis of these results, we conclude that atmospheric circulation anomalies in late spring–early summer (April–June or July) exert a stronger influence upon summer sea ice cover than those in high summer (June–August).

The spatial relation and close temporal correspondence between the late spring SLP and summer ice extent anomaly patterns shown in Figs. 16 and 17 indicate that spring atmospheric circulation anomalies likely initiated the observed summer sea ice cover changes during the past 40 yr. Similar conclusions were reached by Serreze et al. (1995) regarding the low ice cover anomaly during summer 1990, and by Maslanik et al. (1996) for the period of generally low summer ice cover during 1990–95. We note that once ice melt is under way, positive ice–albedo feedback can quickly accelerate ice retreat during the summer months. This mechanism may account for the relatively long delay (longer than that found in winter) between the time of anomalous atmospheric forcing (April–June or July) and the period of maximum ice anomalies (July–September). Positive ice–albedo feedback may also account for the amplification of negative sea ice trends relative to positive ones during 1979–96 (Fig. 17, lower panel), especially considering that the spring SLP anomaly pattern would likely have produced a more balanced pattern of ice anomalies (i.e., larger positive trends in the Greenland, Barents, and Kara Seas due to anomalous northerly winds). Preexisting negative ice trends in winter may also have played a role in reducing the magnitude of the positive summer ice anomalies across the Greenland, Barents, and Kara Seas.

The spring SLP regression maps based upon summer ice extent (Fig. 17) are very similar to those based upon the winter NAO index (not shown), suggesting that spring atmospheric circulation anomalies over the Arctic are tied to winter NAO fluctuations within each subperiod. Note, however, that there is no *consistent* relation between Arctic SLP in late spring and the winter NAO index, since a high NAO winter tends to be followed by high (low) Arctic SLP in late spring during 1958–78 (1979–96). The correlation coefficient between the winter NAO index and the regional summer sea ice extent indices is −0.57 during 1958–78 and −0.65 during 1979–96.

4. Summary and discussion

a. Winter

We have documented the leading pattern of variability of winter (January–March) sea ice concentration anomalies in the Arctic during 1958–97 and its association with surface air temperature and sea level pressure throughout the Northern Hemisphere extratropics. Consistent with previous studies, the dominant structure of sea ice variability (which accounts for 35% of the variance) exhibits out-of-phase fluctuations between the Labrador and Greenland/Barents Seas. A smaller amplitude seesaw occurs in the Pacific sector between the Bering Sea and the Sea of Okhotsk. The time series of the leading EOF exhibits a high winter-to-winter autocorrelation (0.69) and is dominated by decadal-scale variations and a long-term trend of diminishing ice cover east of Greenland and increasing ice cover west of Greenland.

Associated with the dominant pattern of ice variability are large-scale SLP changes reminiscent of the positive polarity of the NAO and AO circulation patterns. The spatial and temporal relationships between

the SLP and ice anomaly fields are consistent with the notion that the atmospheric circulation anomalies force the sea ice variations.

The ice pattern is also associated with hemispheric SAT anomalies: warming over the northern continents and cooling over the subpolar oceans. However, the largest SAT anomalies [10°C (40 yr)$^{-1}$] are coincident with changes in ice cover, with positive SAT anomalies over reduced ice amounts in the Greenland Sea and negative SAT anomalies over enhanced ice cover in the Labrador Sea. The amplification of the SAT perturbations over ice relative to land or ocean results from the strong contrast between ice surface and sea surface temperatures and thus is a direct consequence of the sea ice variations prescribed in the NCEP–NCAR reanalysis.

Consistent with the SAT changes, surface sensible and latent heat flux anomalies are strongly tied to the pattern of sea ice variability, with the largest upward heat flux anomalies [200 W m^{-2} (40 yr)$^{-1}$] directly over the reduced ice cover in the Greenland Sea. The enhanced ocean-to-atmosphere heat and moisture fluxes may have contributed to the observed increase in the number of cyclones over the Greenland Sea. Whether such localized changes in transient eddy activity have any impact upon the atmospheric general circulation through changes in heat and vorticity flux convergence remains to be investigated.

Because the quantitative validity of the reanalysis-derived surface fluxes is open to question, an immediate priority is the use of independent information (e.g., from satellites and field programs) for the assessment and possible improvement of sea ice and surface flux parameterizations in models used to perform atmospheric reanalyses. However, we note that the cyclone statistics used here were determined largely by the directly assimilated SLP data in the atmospheric reanalysis. The assimilated pressure data did not ''know'' that the model's prescribed sea ice was crude and simplistic. In this respect, the cyclone statistics were obtained independently of the sea ice data to which they were compared in this study, and the SLP–sea ice association cannot be considered an artifact of a model that treats sea ice in a questionable manner.

The recent and historically unprecedented trends in the wintertime NAO and AO circulation patterns over the past three decades have been imprinted upon the distribution of Arctic sea ice. The cause of the circulation trends and the sensitivity of the atmospheric flow to the resulting changes in Arctic sea ice are in need of further investigation, especially since feedbacks involving sea ice are likely to shape decade-to-century-scale climate changes in high latitudes.

b. Summer

The dominant mode of sea ice variability in summer is more spatially uniform than that in winter. Summer ice extent for the Arctic as a whole has exhibited a nearly monotonic decline (−4% decade^{-1}) during the past 40 yr. The spatial patterns of ice retreat during the early (1957–78) and late (1979–96) portions of the record differ slightly, with the maximum ice declines located in the Barents, Kara, and Laptev Seas during the early period and in the east Siberian Sea during the later period. Both patterns of summer ice retreat appear to be initiated by atmospheric circulation anomalies over the high Arctic in late spring: Positive ice–albedo feedback may account for the relatively long delay (2–3 months) between the time of atmospheric forcing and the maximum ice response.

An outstanding issue not resolved by our study is why the winter NAO index (or equivalently, a winter SLP pattern index based upon the leading winter sea ice PC) exhibits correlations with spring SLP that are of opposite sign over the high Arctic during the early (1958–78) and late (1979–96) portions of the record. Those opposing spring Arctic SLP anomaly patterns both appear to initiate a net reduction in Arctic summer sea ice cover, but in different areas within the Eurasian coastal waters. We speculate that positive ice–albedo feedback, by amplifying negative sea ice anomalies relative to positive ones, can alter an initially balanced pattern of sea ice changes forced by the atmospheric circulation into one with negative areal mean. Preexisting negative ice anomalies in winter may also have served to reduce the magnitude of positive summer ice anomalies forced by spring atmospheric circulation changes. In this case, winter circulation changes may also be implicated in the summer ice declines.

Acknowledgments. We thank Drs. Mark Serreze and James Maslanik for helpful discussions. We also thank an anonymous reviewer and Professor J. M. Wallace for encouraging us to pursue the summer sea ice variability. Drs. M. Alexander, U. Bhatt, J. Hurrell, S. Peng, D. Thompson, and K. Trenberth provided helpful comments on an earlier version of the manuscript. Dr. Jim Hurrell kindly provided the NAO record. The graphics were produced with the GrADS software package developed by Brian Doty. This study was supported in part by grants from NSF Physical Oceanography ''Atlantic Circulation and Climate Experiment'' to C. Deser and M. Alexander and from NASA Grant POLAR97-0015 to J. Walsh.

APPENDIX

Summer Sea Ice Record

Figure A1 shows the time series of Arctic summer (July–September) sea ice concentrations (%) averaged north of 60°N. The discontinuity between 1978 and 1979 is due to the introduction of satellite passive microwave sensing techniques that depict lower summer ice concentrations within the pack ice.

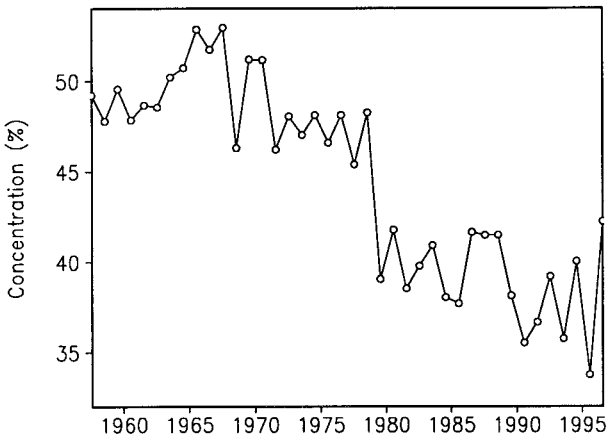

FIG. A1. Time series of Arctic summer sea ice concentrations (%) averaged north of 60°N. The discontinuity between 1978 and 1979 is due to the introduction of satellite passive microwave sensing techniques that depict lower summer ice concentrations within the pack ice.

REFERENCES

Carleton, A. M., 1985a: Synoptic cryosphere–atmosphere interactions in the northern hemisphere from DMSP image analysis. *Int. J. Remote Sens.,* **6,** 239–261.

——, 1985b: Satellite climatological aspects of the ''polar low'' and ''instant occlusion.'' *Tellus,* **37A,** 433–450.

Cavalieri, D. J., P. Gloersen, C. L. Parkinson, J. C. Comiso, and H. J. Zwally, 1997: Observed hemispheric asymmetry in global sea ice changes. *Science,* **278,** 1104–1106.

Chapman, W. L., and J. E. Walsh, 1993: Recent variations of sea ice and air temperature in high latitudes. *Bull. Amer. Meteor. Soc.,* **74,** 33–47.

Dickson, R. R., J. Meincke, S. A. Malmberg, and A. J. Lee, 1988: The ''Great Salinity Anomaly'' in the northern North Atlantic, 1968–1982. *Progress in Oceanography,* Vol. 20, Pergamon Press, 103–151.

Fang, Z., and J. M. Wallace, 1994: Arctic sea ice variability on a timescale of weeks: Its relation to atmospheric forcing. *J. Climate,* **7,** 1897–1913.

Herman, G. F., and W. T. Johnson, 1978: The sensitivity of the general circulation to Arctic sea ice boundaries: A numerical experiment. *Mon. Wea. Rev.,* **106,** 1649–1664.

Hsiung, J., 1986: Mean surface energy fluxes over the global ocean. *J. Geophys. Res.,* **91,** 10 585–10 606.

Hurrell, J. W., 1995: Decadal trends in the North Atlantic oscillation regional temperatures and precipitation. *Science,* **269,** 676–679.

——, 1996: Influence of variations in extratropical wintertime teleconnections on Northern Hemisphere temperature. *Geophys. Res. Lett.,* **23,** 665–668.

——, and H. van Loon, 1997: Decadal variations in climate associated with the North Atlantic Oscillation. *Climatic Change,* **36,** 301–326.

IPCC, 1990: *Climatic Change: The IPCC Assessment.* J. T. Houghton, G. J. Jenkins, and J. J. Ephraums, Eds., Cambridge University Press, 365 pp.

Kalnay, E., and Coauthors, 1996: The NCEP/NCAR 40-yr Reanalysis Project. *Bull. Amer. Meteor. Soc.,* **77,** 437–471.

Lemke, P., E. W. Trinkl, and K. Hasselmann, 1980: Stochastic dynamic analysis of polar sea ice variability. *J. Phys. Oceanogr.,* **10,** 2100–2120.

Manabe, S., M. J. Spelman, and R. J. Stouffer, 1992: Transient response of a coupled ocean–atmosphere model to gradual changes of atmospheric CO_2, Part II: Seasonal response. *J. Climate,* **5,** 105–126.

Maslanik, J. A., M. C. Serreze, and R. G. Barry, 1996: Recent decreases in Arctic summer ice cover and linkagges to atmospheric circulation anomalies. *Geophys. Res. Lett.,* **23,** 1677–1680.

Moritz, R. E., J. A. Curry, N. Untersteiner, and A. S. Thorndike, 1993: Prospectus: Surface heat budget of the Arctic Ocean. NSF-ARCSS OAII Tech. Rep. 3, 33 pp. [Available from SHEBA Project Office, Polar Science Center, Applied Physics Laboratory, University of Washington, Seattle, WA 98105.]

Mysak, L. A., and S. B. Power, 1992: Sea-ice anomalies in the western Arctic and Greenland-Iceland sea and their relation to an interdecadal climate cycle. *Climatol. Bull.,* **26,** 147–176.

——, R. G. Ingram, J. Wang, and A. Van Der Baaren, 1996: The anomalous sea–ice extent in Hudson Bay, Baffin Bay and the Labrador Sea during three simultaneous ENSO and NAO episodes. *Atmos. Ocean,* **34,** 313–343.

NSIDC, 1998: Sea ice concentration datasets. NSIDC Notes No. 24, National Snow and Ice Data Center, Boulder, CO, 1–3. [Available from NSIDC, University of Colorado, Campus Box 449, Boulder, CO 80309-0449.]

Overland, J. E., and C. H. Pease, 1982: Cyclone climatology of the Bering Sea and its relation to cyclone extent. *Mon. Wea. Rev.,* **110,** 5–13.

Parkinson, C. L., D. J. Cavalieri, P. Gloersen, H. J. Zwally, and J. Comiso, 1999: Arctic sea ice extents, areas, and trends, 1978–1996. *J. Geophys. Res.,* **104** (C9), 20 837–20 856.

Prinsenberg, S. J., I. K. Peterson, S. Narayanan, and J. U. Umoh, 1997: Interaction between atmosphere, ice cover, and ocean off Labrador and Newfoundland from 1962–1992. *Can. J. Aquat. Sci.,* **54,** 30–39.

Randall, D., and Coauthors, 1998: Status of and outlook for large-scale modeling of atmosphere–ice–ocean interactions in the Arctic. *Bull. Amer. Meteor. Soc.,* **79,** 197–219.

Rasmussen, E., 1985: A case study of a polar low development over the Barents Sea. *Tellus,* **37A,** 407–418.

Reynolds, R. W., and T. M. Smith, 1995: A high resolution global sea surface temperature climatology. *J. Climate,* **8,** 1571–1583.

Rind, D., R. Healy, C. Parkinson, and D. Martinson, 1995: The role of sea ice in $2\times CO_2$ climate model sensitivity. Part I: The total influence of sea ice thickness and extent. *J. Climate,* **8,** 449–463.

Rogers, J. C., 1990: Patterns of low-frequency monthly sea level pressure variability (1899–1986) and associated wave cyclone frequencies. *J. Climate,* **3,** 1364–1379.

——, and H. van Loon, 1979: The seesaw in winter temperatures between Greenland and northern Europe. Part II: Some oceanic and atmospheric effects in middle and high latitudes. *Mon. Wea. Rev.,* **107,** 509–519.

Sardie, J. M., and T. T. Warner, 1985: A numerical study of the development mechanisms of polar lows. *Tellus,* **37A,** 460–477.

Shuchman, R. A., E. G. Josberger, C. A. Russel, K. W. Fischer, O. M. Johannessen, J. Johannessen, and P. Gloersen, 1998: Greenland Sea Odden sea ice feature: Intra-annual and interannual variability. *J. Geophys. Res.,* **103,** 12 709–12 724.

Serreze, M. C., 1995: Climatological aspects of cyclone development and decay in the Arctic. *Atmos.–Ocean,* **33,** 1–23.

——, J. A. Maslanik, J. R. Key, R. F. Kokaly, and D. A. Robinson, 1995: Diagnosis of the record minimum in Arctic sea ice area during 1990 and associated snow cover extremes. *Geophys. Res. Lett.,* **22,** 2183–2186.

——, F. Carse, R. G. Barry, and J. C. Rogers, 1997: Icelandic low activity: Climatological features, linkages with the NAO, and relationships with recent changes in the Northern Hemisphere circulation. *J. Climate,* **10,** 453–464.

Simmonds, I., and W. F. Budd, 1991: Sensitivity of the southern hemisphere circulation to leads in the Antarctic pack ice. *Quart. J. Roy. Meteor. Soc.,* **117,** 1003–1024.

Slonosky, V. C., L. A. Mysak, and J. Derome, 1997: Linking arctic sea ice and atmospheric circulation anomalies on interannual and decadal time scales. *Atmos.–Ocean,* **35,** 333–366.

Thompson, D. W. J., and J. M. Wallace, 1998: Observed linkages

between Eurasian surface air temperature, the North Atlantic Oscillation, Arctic sea level pressure and the stratospheric polar vortex. *Geophys. Res. Lett.,* **25,** 1297–1300.

——, ——, and G. C. Hegerl, 2000: Annular modes in the extratropical circulation. Part II: Trends. *J. Climate*, in press.

Wallace, J. M., Y. Zhang, and K.-H. Lau, 1993: Structure and seasonality of interannual and interdecadal variability of the geopotential height and temperature fields in the Northern Hemisphere troposphere. *J. Climate,* **6,** 2063–2082.

——, ——, and L. Bajuk, 1996: Interpretation of interdecadal trends in Northern Hemisphere surface air temperature. *J. Climate,* **9,** 249–259.

Walsh, J. E., and C. M. Johnson, 1979: An analysis of arctic sea ice fluctuations, 1953–77. *J. Phys. Oceanogr.,* **9,** 580–591.

——, W. L. Chapman, and T. L. Shy, 1996: Recent decrease of sea level pressure in the central Arctic. *J. Climate,* **9,** 480–486.

Wiese, W., 1924: Polareis und Atmospharische Schwankungen. *Geograf. Ann.,* **6,** 273–299.